A 16×16 Micro Mirror Array for Optical Switches

Chen Qinghua, Wu Wengang†, Wang Ziqian, Yan Guizhen, and Hao Yilong

(*National Key Laboratory of Micro/Nano Fabrication Technology, Institute of Microelectronics, Peking University, Beijing* 100871, *China*)

Abstract: This paper reports on the design, fabrication, and performance of a high-reflectivity large-rotation mirror array for MEMS (micro-electro-mechanical system) 16×16 optical switches. The mirror in the array can enlarge its rotation angles up to 90° and keep a steady state to steer the optical signal. According to the large-rotation behavior, an electromechanical model of the mirror is presented. By monolithic integration of fiber grooves and mirrors fabricated by a surface and bulk hybrid micromachining process, the coarse passive alignment of fiber-mirror-fiber can be achieved. The reflectivity of the mirror is measured to be 93.1%～96.3%. The switches demonstrate that the smallest fiber-mirror-fiber insertion loss is 2.1dB using OptiFocus™ collimating lensed fibers. Moreover, only about ±0.01dB oscillating amplitude of insertion loss is provoked after the device is tested for 15min for 5～90Hz in the vertical vibration amplitude of 3mm.

Key words: optical switch; micro-mirror array; large rotation; electrostatic actuation; MEMS
PACC: 4283; 4225B; 4230Q
CLC number: TN25 **Document code**: A **Article ID**: 0253-4177(2008)08-1496-08

1 Introduction

Micromirrors fabricated by MEMS technologies have been important building blocks for many micro-optical systems[1,2]. Particularly, optical switches are most commonly used. They offer the fundamental advantages exploiting the benefits of free-space interconnection (including low loss and crosstalk, and low polarization- and wavelength-dependence), together with the advantages of integrated optics (including optical pre-alignment, compactness, and low cost).

There are two approaches to achieve MEMS optical switches: two-dimensional (2D) MEMS and three-dimensional (3D) MEMS. The 3D MEMS optical switches are intended to be used as large-scale optical cross-connect systems for backbone networks. Compared to the 3D switches, the 2D MEMS optical switches are better for small- and medium-scale applications and are popular for their reliability and simple packaging.

MEMS 2D optical switches present the challenge of achieving optical-fibers-to-mirrors alignment as precise as possible for low optical loss. The simplest approach is to use external regulating equipment such as silicon submounts to adjust the optical fibers[3～5]. However, the corresponding free space fiber alignment process is highly time-consuming and the fiber positioning accuracy is liable to be influenced by position vibration of the mirrors, particularly in large scale switch arrays.

An efficient solution to the alignment problem is monolithically integrating the fiber grooves and micromirrors. Using accurate photolithography processes and microfabrication techniques, precisely-positioned fiber grooves with only micro-scale aberration can be achieved. Compared to the non-fiber-groove structure, it is very convenient and reliable to align the fibers as a result of the grooves, thus it avoids the pure manual alignment process. In addition, this approach offers high density packaging over optical fibers.

Several MEMS-based mirror structures using this approach have been reported over the past few years[6～9]. Researchers used an etched vertical surface as the mirror element[6,7]. With the convenient DRIE method, a vertical sidewall with 90° can be achieved. However, the challenge of using an etched vertical surface is that it is difficult to use as a mirror for a switch array, even if it remains smooth enough for many micro-mirror applications. Furthermore, it is challenging to sputter a uniform reflective gold coating on the vertical mirror array. A rough surface with inferior metal coating results in scattering losses, which produce crosstalk and increased insertion loss. Thus, the wet anisotropic etching technique was developed to improve the surface quality of the vertical mirrors[8]. These mirrors formed by particular single crystal surface have excellent surface quality. Furthermore, single crystal silicon substrates with high purity are readily available at low cost. However, these mirrors have to be precisely aligned with particular crystal directions, imposing restrictions on the structural

† Corresponding author. Email: wuwg@ime.pku.edu.cn
Received 25 January 2008, revised manuscript received 19 April 2008

design. Thus, only very simple actuator functions are realized. Another approach is fabricating the mirror array from a flat and smooth horizontal reflector surface[9]. A polished single crystal silicon (SCS) surface is employed as the horizontal mirror surface, which has low surface roughness for optical reflection and is convenient for metal sputtering. However, it poses the challenge of preventing the mirror from vibration or oscillation resulting form external turbulence to avoid mishandling.

In this work, we present a 16 × 16 2D optical switch based on electrostatically-driven large-rotation mirrors. This structure monolithically integrates the fiber grooves, and moreover, several goals are achieved simultaneously: First, flat and smooth mirrors are achieved using a horizontal polysilicon layer deposited on an SCS wafer, which offers easy sputtering and lithographically patterning for gold coating. Second, the structural design restrictions are eliminated because it has no demand for the alignment with particular crystal directions. Third, a stable "ON" state for the mirror is obtained using a vertical sidewall as a mechanical stopper to overcome the external turbulence. The reflectivity of the micromirror is measured to be 93.1% ~ 96.3%. The smallest fiber-mirror-fiber insertion loss of 2.1dB has been obtained for OptiFocus™ collimating lensed fibers. Moreover, only about ± 0.01dB oscillating amplitude of insertion loss in the "ON" state is provoked when the device is tested for 15min for 5~90Hz in the vertical direction with a vibration amplitude of 3mm.

2 Operation principles and design

2.1 Micromirror design

The three-dimensional diagram of the optical switch is shown in Fig. 1. Micro mirrors supported by torsion beams across the through-holes are located at the crossings by 45° inclination to the light beams and arranged in a matrix (from $M(1,1)$ to $M(16,16)$) to compose a 16 × 16 optical switch. In this work, the mirror with the shortest total distance between the mirror and the two fibers is defined as $M(1,1)$ while the one with the longest distance is defined as $M(16,16)$. When transmitting to the mirror elements through the cross deep grooves, the incident light beams can propagate in their original directions without interruption under the horizontal "OFF" micromirrors and can be reflected by the vertical "ON" micromirrors. Accordingly, a compact optical switch device can be achieved since the light beams can crisscross each other in free-space without interference.

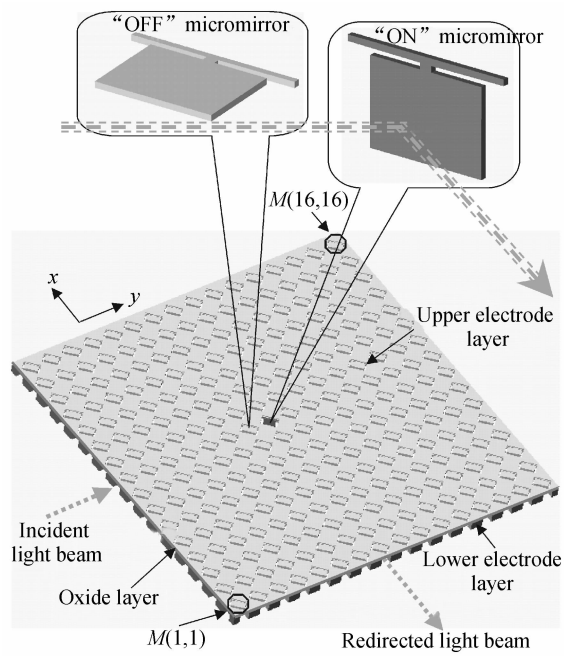

Fig. 1　Three-dimensional schematic of the 16 × 16 optical switch

Figure 2 illustrates the electrostatic operation principle of the optical switch. Initially, both the vertical sidewall electrodes and the mirror plates are held at ground potential. The mirrors are in the "OFF" state and all the mirror plates are horizontal [see Fig. 2(a)]. During a switching event, the movable mirror to rotate downwards is subjected to an electrostatic force when its potential is biased, and the rotating angle of the mirror increases with the driving voltage. Simultaneously, inactive mirrors remain horizontal to avoid blocking the optical beams [see Fig. 2(b)]. Once the driving voltage increases to the pull-in voltage $V_{\text{pull-in}}$, the mirror switches to the "ON" state, which is captured and clamped to the vertical sidewalls [see Fig. 2(c)]. Then, the amplitude of the driving voltage keeping the mirror in the "ON" state can be reduced to the lower V_{hold} because the electrostatic force overcomes the torsion spring torque. When the mirror potential is set to ground potential, it releases the electrostatic clamping force and allows the torsion spring torque to pull the mirror away from the vertical place to the horizontal place [see Fig. 2(d)].

2.2 Mechanical design

One of the most important design problems in structural design is the coupling of the mechanics and the electrostatics, which governs the behavior of the mirror.

The actuator model is illustrated in Fig. 3. The actuator is constructed from a top horizontal plate electrode and a fixed vertical sidewall electrode. The

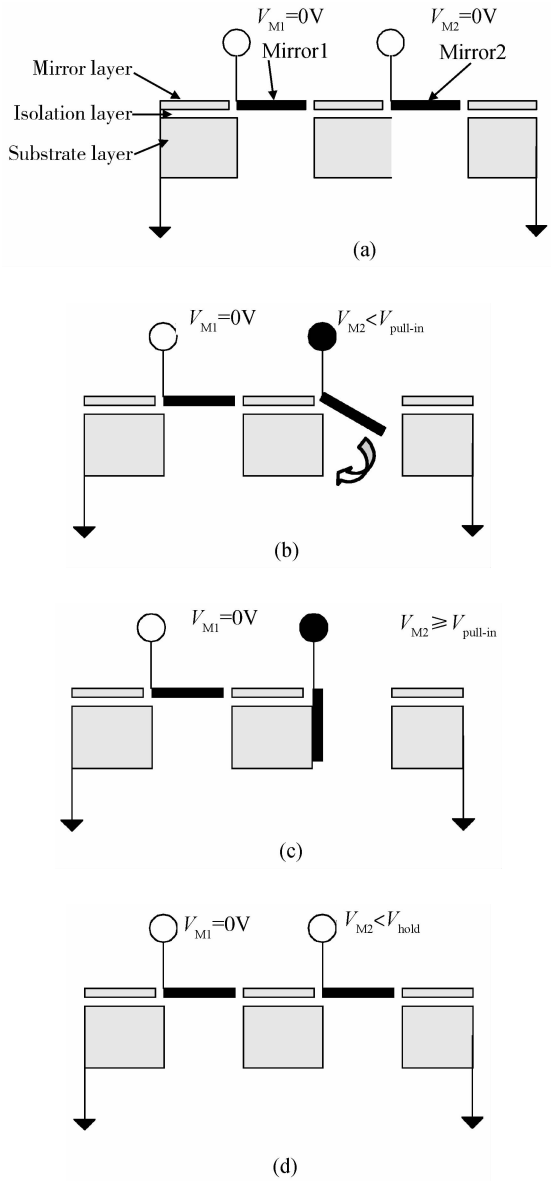

Fig. 2 Cross-sectional view of the switch device illustrating the electrostatic actuation principle (a) In the OFF state, all mirrors are grounded along with the substrate layer; (b) Mirrors that are to be switched rotate to the substrate sidewall by applying the driving voltage to the mirrors, while mirrors that are kept horizontal remain grounded; (c) Mirrors are clamped to the sidewall and switch to the ON state when the driving voltage reaches $V_{pull-in}$; (d) Mirrors return to the OFF state when the applied voltage is less than V_{hold}

fixed vertical electrode is electrically grounded and the micromirror can deflect downwards to the vertical sidewall electrode due to the electrostatic torque and force resulting from driving voltage V.

To obtain straightforward insight into the mirror deflection, modal analysis has been performed using ANSYS software. The self-deformation of the micromirror plate is very small, thus, the micromirror can be regarded as a rigid body. Based on this simulation, we make two assumptions to simplify the calculation in this model: (1) The distribution of the electrostatic field is uniform along the axis parallel to the torsion beams, and thus we consider the mirror as a part of an infinite ribbon; (2) The shape of the field is represented by the arc whose pivot is at the intersection of the virtually extended mirror and the vertical sidewall electrode.

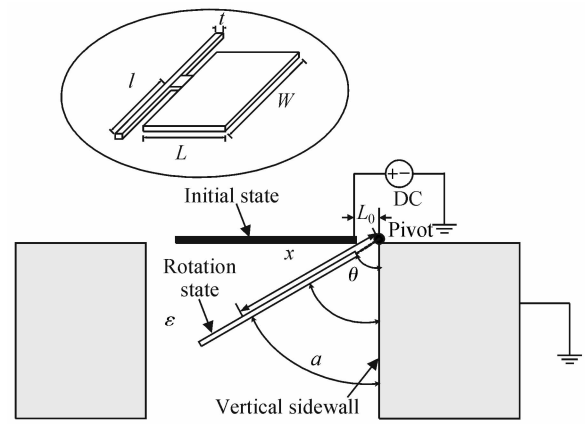

Fig. 3 Analytical model of the large-angular mirror-sidewall actuator

The magnitude of the electrostatic field along the mirror is

$$E = \frac{V}{a} \tag{1}$$

where $a = x\theta$, θ is the angle between the mirror plate and the vertical sidewall electrode, x is the distance to the pivot, and V is the voltage applied to the mirror electrode.

Then, the electrostatic pressure along the mirror is

$$P = \frac{\varepsilon E^2}{2} \tag{2}$$

where ε is the dielectric constant of the vacuum.

By integrating the electrostatic torque $xPW\mathrm{d}x$ over $x = [L_0, L + L_0]$, we obtain the total torque by electrostatic attraction.

$$T_e = \int_{L_0}^{L_0+L} xPW\mathrm{d}x \approx \frac{\varepsilon^2 V^2 W}{2\theta^2}\ln\frac{L}{L_0} \tag{3}$$

where L_0 is the distance between the pivot and the right end of the mirror, and W and L are the width and length of the mirror plate, respectively. In Eq. (3), we assume that $L + L_0 \approx L$, since L_0 is relatively much smaller than L.

On the other hand, the spring restoring torque, T_s, provided by the torsion hinges, is defined as follows.

$$T_s = k_\theta\left(\frac{\pi}{2} - \theta\right) \tag{4}$$

where

$$k_\theta = 2 \times \frac{Gwt^3}{3l}\left\{1 - \frac{192}{\pi^5} \times \frac{t}{w}\tanh\left(\frac{\pi w}{2t}\right)\right\} \approx 2 \times \frac{Gwt^3}{3l}$$

w, l, and t are the width, length, and thickness of the torsion beam, respectively, and G is the shear modulus

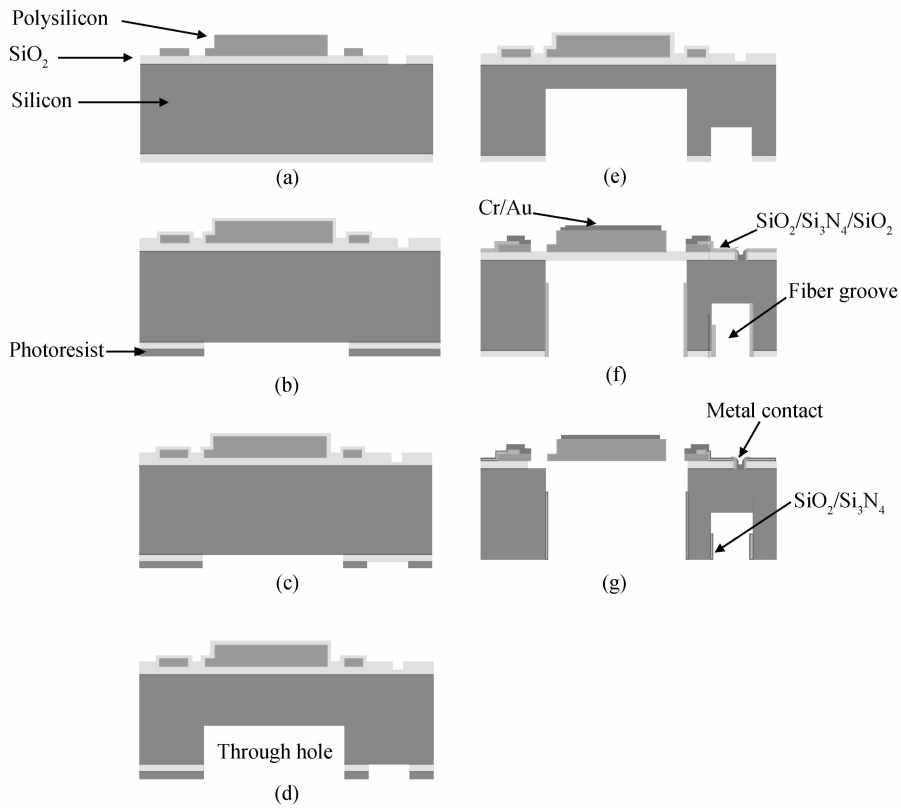

Fig. 4　Fabrication process flow of the optical switch

of polysilicon. We assume the first term of k_θ represents the total k_θ since it is much larger than the second term, which simplifies the numerical calculation.

When in the steady state, the expression for V as a function of θ can be established by the equilibrium between T_e and T_s, as shown in the following equations.

$$V = \sqrt{\frac{4Gwt^3\theta^2}{3\varepsilon lW\ln\dfrac{L}{L_0}}\left(\frac{\pi}{2}-\theta\right)} \tag{5}$$

Electrostatic pull-in occurs for the torsion mirror when the nonlinear electrostatic torque overwhelms the available restoring torque. The pull-in voltage V_{PI} of the electrostatic actuator can be calculated as

$$V_{PI} = \frac{\pi^{3/2}}{9}\sqrt{\frac{2Gwt^3}{3\varepsilon lW\ln\dfrac{L}{L_0}}} \tag{6}$$

The influence of parameter t on both V and V_{PI} is the most significant of the controllable structural parameters. Therefore, thinning the thickness of the torsion beam can effectively lower the driving voltage. Based on a compromise between performances and fabrication considerations, the thickness of the torsion beam is set to 1.5μm. The other structural parameters of the designed structure are listed in Table 1.

3　Fabrication

The present process consists of eight photolithography masks; six front-side masks for the mirror structure, contact windows, metal pads; and two back-side masks to construct the designed vertical sidewalls and fiber grooves.

The simplified process flow of the switch is shown in Fig. 4. The process begins with the deposition of the 1.6μm silicon oxide and 2μm polysilicon on a (100)-oriented n-type SCS wafer. The oxide insulates the polysilicon layer, which serves as a device layer from the SCS substrate. Then the polysilion layer is patterned using a reactive ion etching (RIE) process to define mirror shape (mask #1) and the torsion beam (mask #2). After that, the contact windows are patterned (mask #3) and opened by RIE

Table 1　Physical parameters of the mirror design physical meaning value

l	Length of torsion beam	760μm
w	Width of torsion beam	5μm
t	Thickness of torsion beam	1.5μm
L	Length of mirror	360μm
W	Width of mirror	600μm
L_0	Distance between the pivot and mirror	20μm
E_{poly}	Young's modulus of polysilicon	1.69×10^5GPa
ν	Possion ration of polysilicon	0.066
ε	Dielectric constant of the vacuum	8.854pF/m

etching (Fig. 4(a)). The polysilicon torsion beam is thinned to 1.5μm, which is thinner than the mirror (2μm), to decrease the driving voltage.

Subsequently, the backside deposited polysilicon layer is removed by RIE, followed by deposition of 0.4μm silicon oxide to protect the front-side mirror surface from wear during the subsequent processes. The backside oxide is then patterned (mask #4) and etched to define the through-hole area (Fig. 4(b)). Once the photosensitive resist (PR) is removed, another PR patterning (mask #5) is employed on the backside of the wafer. Thus, a composite etching mask composed of PR and oxide is established for the deep reactive ion etching (DRIE) process (Fig. 4(c)). The first DRIE step is to form the through-hole structure. This step is completed when the etch depth reaches the desired height of 160μm. Then, an RIE process is used to etch the deposited oxide exposed on the backside without PR covering (Fig. 4(d)). The latest exposed silicon regions are prepared to produce the optical fiber grooves. The second DRIE is timed to leave 60μm between the bottom of the trenches and the oxide layer, which can secure the mirrors from cracking (Fig. 4(e)). Due to the high-aspect ratio DRIE, the resulting fiber grooves and vertical sidewalls are fabricated with precise alignment.

Subsequently, a sandwich layer consisting of $SiO_2/Si_3N_4/SiO_2$ is deposited for isolation and then selectively removed from the mirror and electrode regions on the front side (mask #6). This is required for creating proper silicon regions for metal contacts.

Then, a Cr/Au layer is deposited by sputtering and patterned (mask #7 and mask #8) to form lead wire, metal pads, and high-reflectivity surfaces on the micromirrors (Fig. 4(f)). For very small lead wire separation, the electrical wires do not overlap but a misconnection might occur due to the metal lift-off process. Therefore, the wire separation should be adequately designed for wire fabrication. However, if the separation of the wires is too large, the large optical transmission distance is followed by increasing the spacing between the mirrors. For the designed mirror array, as reported here, the minimum wire separation has a value of about 25μm, which can guarantee the lift-off process and minimize the spacing of the mirrors. The third backside DRIE is done until the through-hole reaches the oxide layer.

Finally, a HAC and NH_4F compositing wet-etching process is carried out for 30min to release the micromirrors by eliminating the whole underlying oxide (Fig. 4(g)). The previously deposited Si_3N_4 film of the sandwich layer is selected as a protective layer for the oxide on the sidewalls due to the large expected etching speed ratio between oxide and Si_3N_4. Thus, the remaining oxide and Si_3N_4 layers are used together as an insulation layer to avoid breakdown when the micromirrors touch the vertical sidewalls.

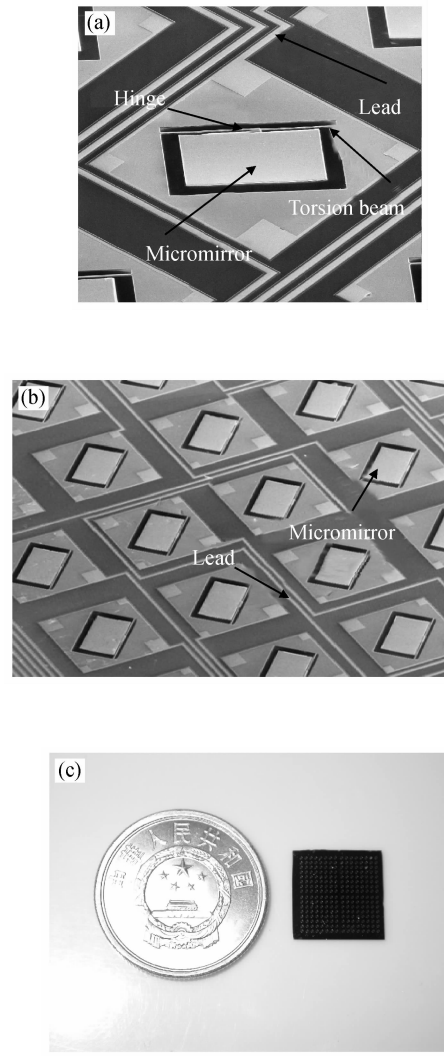

Fig. 5 Images of the optical switch (a) Close-up SEM view of the fabricated micromirror structure; (b) Local SEM view of the optical switch; (c) Dimension view of a whole optical switch

4 Results and measurements

The SEM views of the optical switch are shown in Fig. 5. Figure 5(a) shows a close-up SEM image of a fabricated micromirror covered with Au. The measured dimension of the mirror is 360μm × 600μm, and the torsion spring is 760μm long and 5μm wide. Figure 5(b) shows a local SEM view of an optical switch. The optical switch has 256 micromirror elements and each is separated by lead wires. Figure 5(c) shows a dimensional view of a whole optical switch. In this work, the measurements were performed on eight representative switches selected randomly from the dozens of obtained devices.

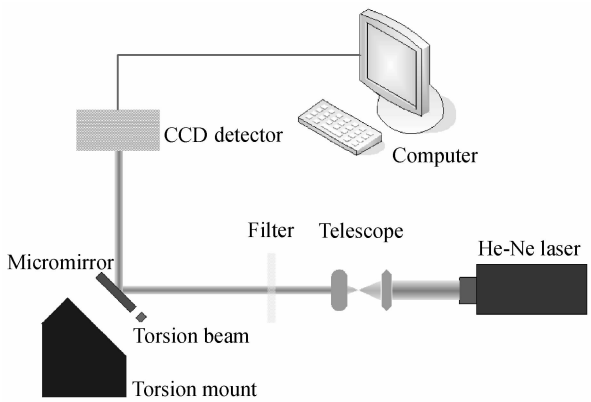

Fig. 6　Configuration of experiment for electromechanical performance

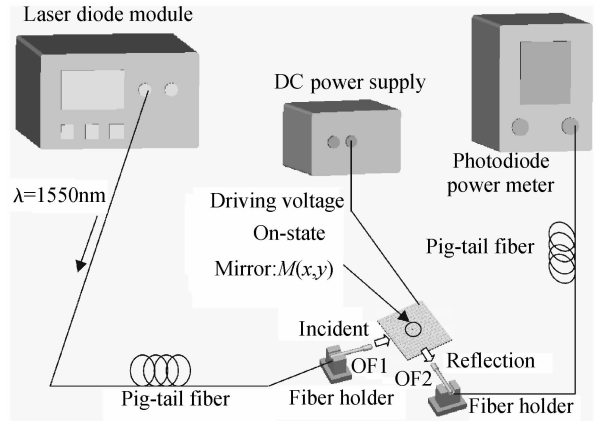

Fig. 8　Configuration of optical switching experiment

4.1　Electromechanical performance

First, the electromechanical performance of the micromirrors was examined experimentally. The experimental setup is shown in Fig. 6. The optical beam from a He-Ne laser is reduced by a telescope to 0.16mm in diameter to be completely covered by the micromirror. The incident optical beam is horizontal and the optical switch is placed on a fixed sloping mount. The profiles of the optical beam are recorded by a CCD detector that can measure the shifts of the beam reflected by micromirrors and processed by a computer. A neutral density filter is used to prevent CCD from saturation.

In Fig. 7, the curve with circular dots shows the typical measured angular motion of the mirror as a function of applied DC voltage, and the dashed line represents the theoretical behavior of the mirror when the voltage is larger than the pull-in value.

Spontaneous electrostatic pull-in behavior of the mirror is observed at a driving voltage of 208V, where the rotation angle 27° is the maximum stable angle in the actuation. In spite of such large-rotation operation, the measured result is found to be in fine agreement with the theoretical analysis, and the difference between theoretical and experimental pull-in voltage is within 10%. In order to avoid being permanently stuck, adequate stiffness of the torsion beam and an anti-friction structure to reduce the interface should be employed. Furthermore, sufficient isolation coating is of critical importance to prevent dielectric breakdown between the mirror layer and substrate, particularly when the micromirror contacts the vertical sidewall. In this work, 400nm SiO_2 and 150nm Si_3N_4 deposition films are introduced to meet the operation requirement, which can endure more than 300V. In addition, the micromirror in the pull-in state does not leave the vertical sidewall until the holding voltage is lower than 20V.

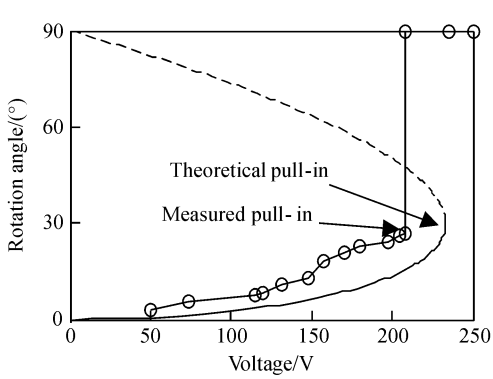

Fig. 7　Comparison of the experiment results with the theoretical results of optical mirror structures

4.2　Optical performance

One of the most important parameters for optical switches for optical communication is the insertion loss in the coupling system consisting of the mirror, input fiber end, and output fiber. Commercially standard single mode fibers (OptiFocus™ Pro. 700043) with a special ball lens fused at the facets of the fiber ends are used as the input and output fibers to reduce the light diffraction from the input fiber end and, simultaneously, enhance the light collection at the output fiber end.

The schematic measurement system is shown in Fig. 8. After the passive optical alignment for the fibers is implemented using the fiber grooves, the light beam from the laser diode module, which exhibits a central wavelength of 1550nm, is introduced to the incident optical fiber (OF1). When the driving voltage reaches the pull-in value, the switch switches to the ON state to perform the reflection function. Afterwards, active optical alignment is employed. The incident light beam is aligned to the mirror $M(x, y)$ using a manually controlled fiber holder such that the redirected beam is coupled into the receiving fiber, OF2, which is detected with a photodiode power me-

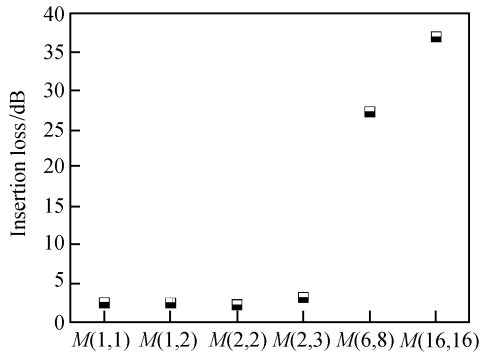

Fig. 9 Experimental results of insertion loss for six mirrors

ter. Other mirrors are also tested in the same manner. Experimental results of the insertion loss of the six mirrors are shown in Fig. 9. The obtained insertion losses range from 2.1 to 37.1dB. The insertion loss includes not only the transmission loss, but also the scattering loss from the polysilicon surface and the loss due to the slight curvature of the mirror. Generally, the insertion loss increases with the subscript of the mirror. For the element $M(16,16)$, which has the longest optical path, the insertion loss is quite large. This is because the input light beam is scattered drastically along with the optical path, which is larger than 15mm. This problem can be effectively solved by assembling the microballs into the substrate, and the cavity holding the microball can be fabricated in the same process as in this work.

With pure passive optical alignment using the fiber grooves, the minimum optical insertion losses are much higher ($>$16dB) for the reflection state. The primary insertion loss is attributed to the residue angular misalignment caused by the variation of diameters and shapes of the special ball lenses. The variation from the designed value causes the input beam to deflect and thus, a very limited optical beam can reach the output fibers. The impact of angular misalignment can be minimized by improving the special ball lenses with more accurate and uniform diameters, properly increasing the diameters of the ball lenses, and reducing the working distance (the total distance between the fibers). For low-cost fiber-optic switches, fiber grooves with passive alignment are still attractive as a developing trend. In addition, the reflectivity of the micromirror is measured to be 93.1% ~96.3%.

4.3 Optical performance in vibration environment

To test device behavior when subjected to vibration during operation as set forth in the vibration table for a common environment, the change in insertion loss was measured under an initial insertion loss due to application of pull-in voltage. The device was tested for 15min for 5~90Hz in the vertical direction with a vibration amplitude of 3mm. The results show no significant difference in the insertion losses, and the characteristics are extremely stable——only about $\pm$0.01dB with an insertion loss of approximately 2.1dB. Thus, the device can effectively endure vibration or oscillation resulting form external turbulence.

5 Conclusion

We have designed and fabricated a MEMS 16×16 optical switch with large-rotation high-reflectivity mirrors actuated by vertical sidewall actuators. Using high-quality mirrors and monolithic integrated fiber grooves, passive alignment is achieved. The reflectivity of the mirror is measured to be 93.1% ~96.3%. The smallest fiber-mirror-fiber insertion loss is 2.1dB using OptiFocus™ collimating lensed fibers. Moreover, only about $\pm$0.01dB oscillating amplitude of insertion loss was provoked when the device was tested for 15min with 5~90Hz and with 3mm vibration amplitude in the vertical direction. In addition, excellent anti-fatigue performance of the mirror structure, which can endure more than 10^9 cycles of actuation, has been proven by fatigue testing.

References

[1] Zhao Y, Tay F E H, Zhou G, et al. A study of electrostatic spring softening for dual-axis micromirror. Optik-International Journal for Light and Electron Optics, 2006, 117(8): 367

[2] Ko Y C, Cho J W, Mun Y K, et al. Eye-type scanning mirror with dual vertical combs for laser display. Sensors and Actuators A: Physical, 2006, 126(1): 218

[3] Lee S S, Huang L S, Kim C J, et al. Free-space fiberoptic switches based on MEMS vertical torsion mirrors. J Lightwave Technol, 1999, 17: 7

[4] Thielicke E, Obermeier E. New MOEMS-switch device with electrostatic actuator. Proc IEEE/LEOS International Conference, 2002: 159

[5] Wood R L, Mahadevan R, Hill E. MEMS 2-D matrix switch. Proc Optical Fiber Communications Conference, Anaheim, CA, 2002: 91

[6] Marxer C, Thio C, Grétillat M A, et al. Vertical mirrors fabricated by deep reactive ion etching for fiber-optic switching applications. J Microelectromechan Syst, 1997, 6(3): 277

[7] Li J, Zhang Q X, Liu A Q. Advanced fiber optical switches using deep RIE (DRIE) fabrication. Sensors and Actuators A, 2003, 102: 286

[8] Helin P, Mita M, Bourouina T, et al. Self-aligned micromachining process for large-scale, free-space optical cross-connects. J Lightwave Technol, 2000, 18(12): 1785

[9] Toshiyoshi H, Miyauchi D, Fujita H. Electromagnetic torsion mirrors for self-aligned fiber-optic crossconnectors by silicon micromachining. IEEE J Sel Topics Quantum Electron, 1999, 5(1): 10

16×16 光开关微镜阵列

陈庆华　吴文刚†　王子千　闫桂珍　郝一龙

（北京大学微电子学与固体电子学研究院 微米/纳米加工技术国家级重点实验室，北京　100871）

摘要：设计、制造和测试了一种实现 16×16 MEMS 光开关的高反射率、大角度静电扭转制动型微镜阵列.该阵列的微镜可进行 90°扭转并保持稳定的扭转状态以对入射光进行导向.针对微镜的扭转驱动特性，提出了相应的机电模型.通过单片集成光纤槽，实现了光纤-微镜-光纤的无源对准.测试结果表明，微镜反射率为 93.1%～96.3%，最低插入损耗为 2.1dB，另外，在经过 15min 的 5～90Hz，3mm 振幅的振动测试后，光开关的插入损耗的改变值仅为 ±0.01dB.

关键词：光开关；微镜阵列；大角度；静电驱动；微电机系统

PACC：4283；4225B；4230Q

中图分类号：TN25　　**文献标识码**：A　　**文章编号**：0253-4177(2008)08-1496-08

† 通信作者.Email：wuwg@ime.pku.edu.cn

2008-01-25 收到，2008-04-19 定稿